Influence of TiB_2 nanoparticles on the elevated-temperature properties of Al-Mn-Mg 3004 alloy

K. Liu *, A. M. Nabawy, X.-G. Chen

Department of Applied Science, University of Quebec at Chicoutimi,

555, Boul. de l'Universite, Saguenay, QC, Canada G7H 2B1

* Corresponding author: kun.liu@uqac.ca, Tel.: 1-418-5455011 ext. 7112; Fax: 1-418-5455012

Abstract:

In the present work, two contents (1.5 wt. % and 3 wt. %) of TiB_2 nanoparticles have been introduced in Al-Mn-Mg 3004 alloy to study their effect on the elevated-temperature properties. Results show that TiB_2 nanoparticles were mainly distributed in the interdendritic grain boundaries with a size range of 20-80 nm, which is confirmed by Transmission Electron Microscopy (TEM) and X-ray diffraction (XRD). Therefore, the volume fraction of the dispersoid free zones is greatly reduced and the motion of grain boundaries and dislocations is inhibited more effectively at elevated temperate. After peak precipitation treatment, the yield strengths in the alloy with 3% TiB_2 addition at room temperature and 300 ^oC were increased by 20% and 13% respectively while the minimum creep rate at 300 ^oC was reduced 5 times compared with the base alloy free of TiB_2, exhibiting a considerable improvement of elevated-temperature properties in Al-Mn-Mg alloys.

Keywords: Al-Mn-Mg 3004 alloy; TiB_2 nanoparticle; Dispersoid free zone; Elevated temperature; Creep resistance.

1. Introduction

Recently, Al-Mn-Mg 3xxx alloys have been developed as one of the most promising candidates in light alloys for the elevated-temperature applications (250 -350 ^oC) due to the formation of thermally-stable dispersoids after proper heat treatments [1-3]. During heat treatment, the dispersoids can precipitate to increase the alloy properties. Meanwhile, the dispersoid free zone (DFZ) is always present in the interdendrites due to the depletion of Mn by forming the Mn-containing intermetallics during the solidification, resulting in a decrease

Foundation item: Natural Sciences and Engineering Research Council of Canada (NSERC) and Rio Tinto Aluminum through the NSERC Industry Research Chair in the Metallurgy of Aluminum Transformation at University of Quebec at Chicoutimi

Corresponding author: Kun Liu; Tel: +01-4185455011 ext. 7112; Fax: +01-4185455012; Email: kun.liu@uqac.ca

of the properties [2]. Therefore, optimizing the dispersoid distribution and controlling the DFZ are two key factors to improve the elevated-temperature properties. Many works have been performed aiming to increase the volume fraction of dispersoids and control their size through modifying the alloying elements or/and the heat treatments [2, 4-6]. Muggerud *et al.* [5] reported that increasing Mn and Si can enhance the precipitation of dispersoids while various heat treatments have been performed to study their influence on dispersoids by Huang *et al.* [4]. However, the balance between dispersoids and DFZ is hard to control. Due to the high precipitation temperature of dispersoids [2], a large volume fraction of DFZ often forms at the peak precipitation condition. On the other hand, DFZ can be decreased by modifying the heat treatment but the size of dispersoids may become bigger with lower volume fraction of dispersoids than their peak condition [5, 7]. Therefore, how to control the DFZ in the microstructure is a significant concern on further improving the elevated-temperature properties of 3xxx alloys.

Introducing the ceramic particles that can be presented at the interdentritic area is one potential approach to decrease the volume fraction of DFZ. The transition metal ceramics are one of them, such as TiC and TiB_2, which are reported to be preferentially located in interdentritic regions during solidification [8, 9]. Meanwhile, it is reported that the addition of high volume of metal ceramic particles to aluminum alloys can improve their alloy properties [10-12]. For instance, the stiffness and ductility has been increased in 1xxx alloys due to the addition of 10% TiB_2 particles [8]. Besides, the creep resistance of the composite has been also increased by two orders of magnitude higher than that of pure aluminum due to the addition of 20% ceramic particles, including SiC, Al_2O_3 and TiB_2 [12].

However, the fabrication difficulties and cost significantly rise with increasing volume fraction of metal ceramic particles due to the poor wettability between them and liquid aluminum. Besides, the size of ceramic particles in the conventional particle-reinforced metal matrix composites is quite big, which often ranges from several μm to few tens μm, limiting the strengthening effect on aluminum matrix [8, 12]. Furthermore, limited open literature in 3xxx alloys about the influence of nanoparticles on properties, especially at elevated temperature, were reported. Therefore, relatively low volume fraction of TiB_2 nanoparticles (1.5-3 wt. %) were introduced to Al-Mn-Mg 3004 alloy in the present work aiming to discover their impact on the elevated-temperature strength and creep resistance.

2. Experimental

Three alloys have been designed in the present work and their nominal compositions are shown in Table 1 (all alloy compositions are shown in wt. % unless indicated otherwise). Two contents of TiB_2 nanoparticles (1.5% and 3%) have been added to the liquid aluminum by flux-assisted melt stirring process [9]. The TiB_2 powder and the K_2ZrF_6 flux were mechanically mixed with a ratio of 1:3 in a ball milling unit and then the powder mixture was pressed to a cylindrical perform. The Al-Mn-Mg base alloy was prepared with pure Al, pure Mg, Al-50%Si, Al-25%Mn and Al-25%Fe master alloys and melted at 850 °C in an electrical resistance furnace. When the melt is ready, the prepared cylindrical perform of powder mixture was added to the melt under mechanical stirring at 900 rpm for 10 minutes. Then the melt was skimmed, poured and solidified in a steel mold preheated at 450 °C. The details about alloy preparation and casting process parameters can be found in our previous work [2, 9].

Table 1 Nominal chemical compositions of alloys used in present work (wt. %)

Alloy Code	Mn	Mg	Fe	Si	TiB_2	Al
B	1.1	1.0	0.6	0.25	***0***	Bal.
T15	1.1	1.0	0.6	0.25	***1.5***	Bal.
T30	1.1	1.0	0.6	0.25	***3***	Bal.

In order to reach the peak precipitation condition, a low temperature heat treatment (375°C for 48h) followed by water quench was adopted on all experimental alloys [2]. The yield strengths (YS) at both room temperature (RT) and 300 °C have been measured in the compression tests performed on a Gleeble 3800 thermomechanical testing unit using the cylindrical specimens with a size of 15 mm in length and 10 mm in diameter. The total deformation of the specimen was set to 0.2, and the strain rate was fixed at 10^{-3} s^{-1}. For the compression test at 300 °C, the specimen was heated to 300 °C with a heating rate of 2 °C/s and held for 3 minutes to stabilize. An average value of YS was obtained from 3 tests. In addition, the compressive creep tests were performed at 300 °C and the specimens were the same size as the Gleeble samples. Creep behaviors were first tested at a constant load of 38 MPa and then multiple loads have been applied to calculate the creep threshold stress and stress exponent. For each condition, 3 tests were repeated to confirm the reliability of the results.

The microstructural features, including characters of TiB_2 nanoparticles, intermetallics, dispersoids and grain structures in both as-cast and heat-treated conditions were observed by

X-ray diffraction (XRD), optical microscope (OM) and electron microscopes. To reveal the dispersoids clearly, the polished samples were etched in 0.5% HF for 30 seconds. A scanning electron microscopy (SEM) equipped electron backscatter diffraction (EBSD) was used to examine the grain structure of alloys. A transmission electron microscopy (TEM) operated at 200 kV was used to observe the distribution of TiB_2 nanoparticles and dispersoids. In this study, the volume fraction of DFZ was converted from the area fraction of DFZ measured in image analysis from optical images according to the Delesse's principle [13]. The volume fraction of dispersoids (V_d) was calculated according to the model introduced in the literature [6] and shown in Eq. (1):

$$V_d = A_d \frac{D}{KD + t}(1 - A_{DFZ}) \quad (1)$$

Where D is the average equivalent diameter of dispersoids, which is calculated according to the literature [6]; t is the TEM foil thickness measured with electron energy loss spectroscopy (EELS); A_d is the area percentage of dispersoids from TEM observation; A_{DFZ} is the area percentage of DFZ from OM measurements; and K is the average shape factor of dispersoids [6] .

3. Results and Discussion

3.1 As-cast and Heat-treated microstructure with various contents of TiB_2 nanoparticles

In order to show the general distribution of TiB_2 particles in alloys, Fig. 1 illustrates the as-cast microstructure of Alloys B, T15 and T30. In the base alloy (Alloy B, Fig. 1a), it can be seen that the microstructure is composed of α-Al cells/grains surrounded with $Al_6(MnFe)$ intermetallic particles [2, 3]. With the addition of TiB_2 nanoparticles in Alloys T15 and T30, those nanoparticles preferentially occurred in the interdendrite regions. As shown in Figs. 1b and 1c, TiB_2 nanoparticles are always present with interdendritic intermetallics. Besides, the volume fraction of nanoparticles remarkably increases in Alloy T30 compared with Alloy T15.

Fig. 2 displays the XRD analysis of experimental alloys in as-cast condition. Compared with the base alloy of Alloy B, there are more peaks appeared in Alloys T15 and T30 besides the peaks of $Al_6(MnFe)$ [14]. According to the literature [15, 16], these additional peaks are identified from the TiB_2 particles, confirming the presence of TiB_2 nanoparticles in solidified microstructure of Alloys T15 and T30. Besides, it seems that the peak intensity of

TiB_2 increases from Alloy T15 to Alloy T30, as shown in dashed box, indicating the higher volume fraction of TiB_2 nanoparticles in Alloy T30 than in Alloy T15.

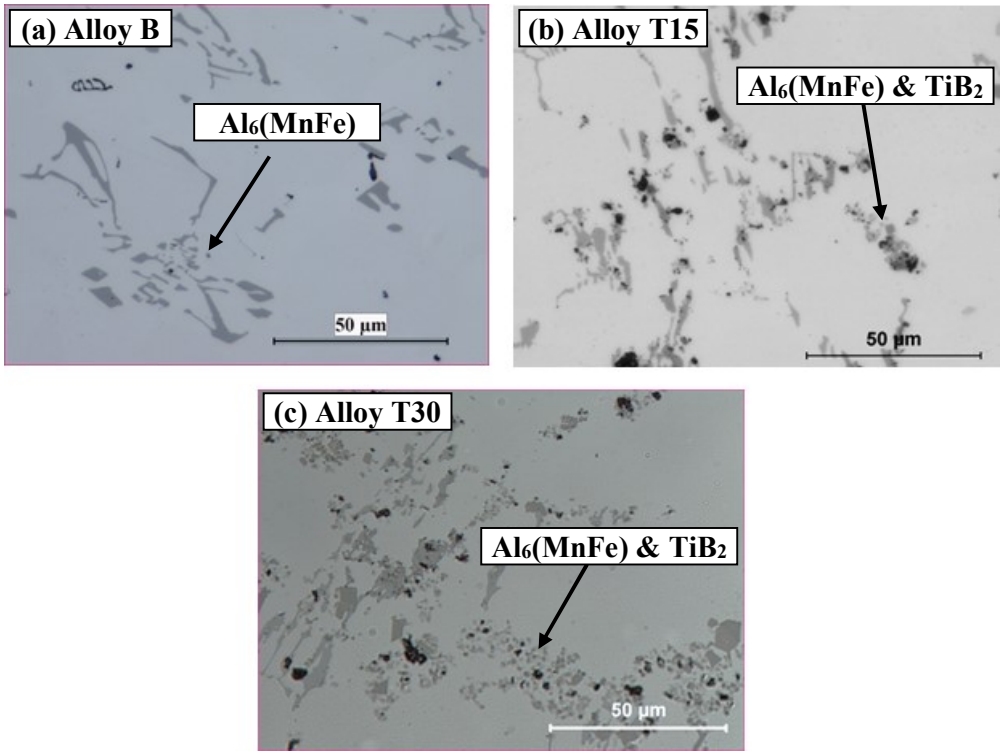

Fig. 1 As-cast microstructure of Alloy B (a), Alloy T15 (b) and Alloy T30 (c)

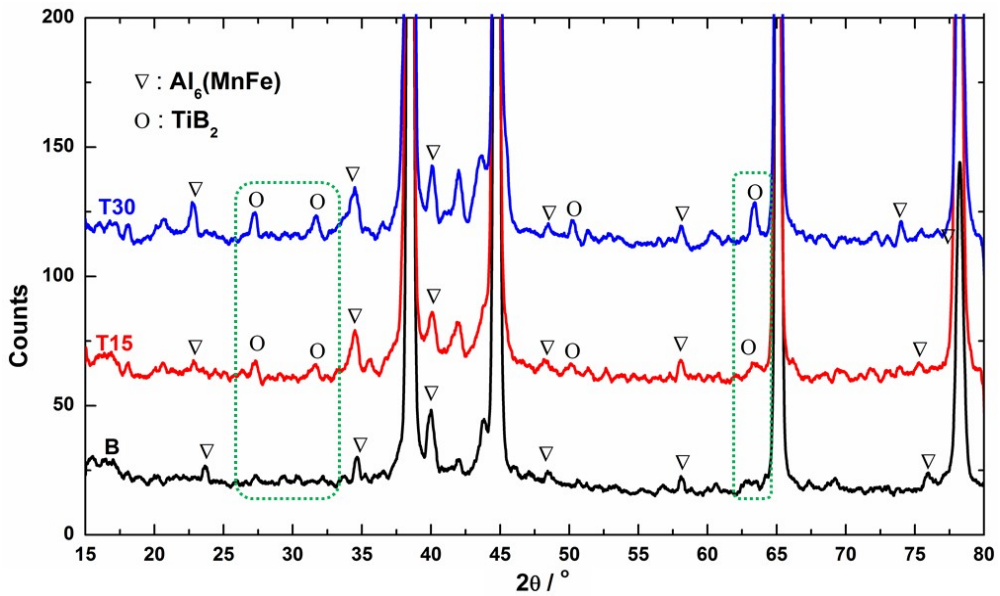

Fig. 2 XRD results of experimental alloys in as-cast condition

Furthermore, TEM is used in the present work to study the incorporation and distribution of TiB2 nanoparticles. As an example, the TEM observation of Alloy T30 with 3% TiB_2 in as-cast condition is displayed in Fig. 3. It can be found in Fig. 3a that the TiB_2

particles are successfully incorporated into aluminum in the form of either cluster or single particles, which is much clear in the enlarged area shown in Fig. 3b. In Fig. 3b, major particles present as single particle with overlaps between them and the size of these particles is in the range of 20-80 nm. Besides, Fig. 3c shows the TEM-EDS result of the particle "A" in Fig. 1b. It can be seen that the particles is composed of Al, Ti and B, confirming the particles as TiB_2 nanoparticles. In addition, the well-indexed selected area diffraction pattern (SADP) from TEM further identify the particle as the hexagonal close-packed (hcp) TiB_2 [17].

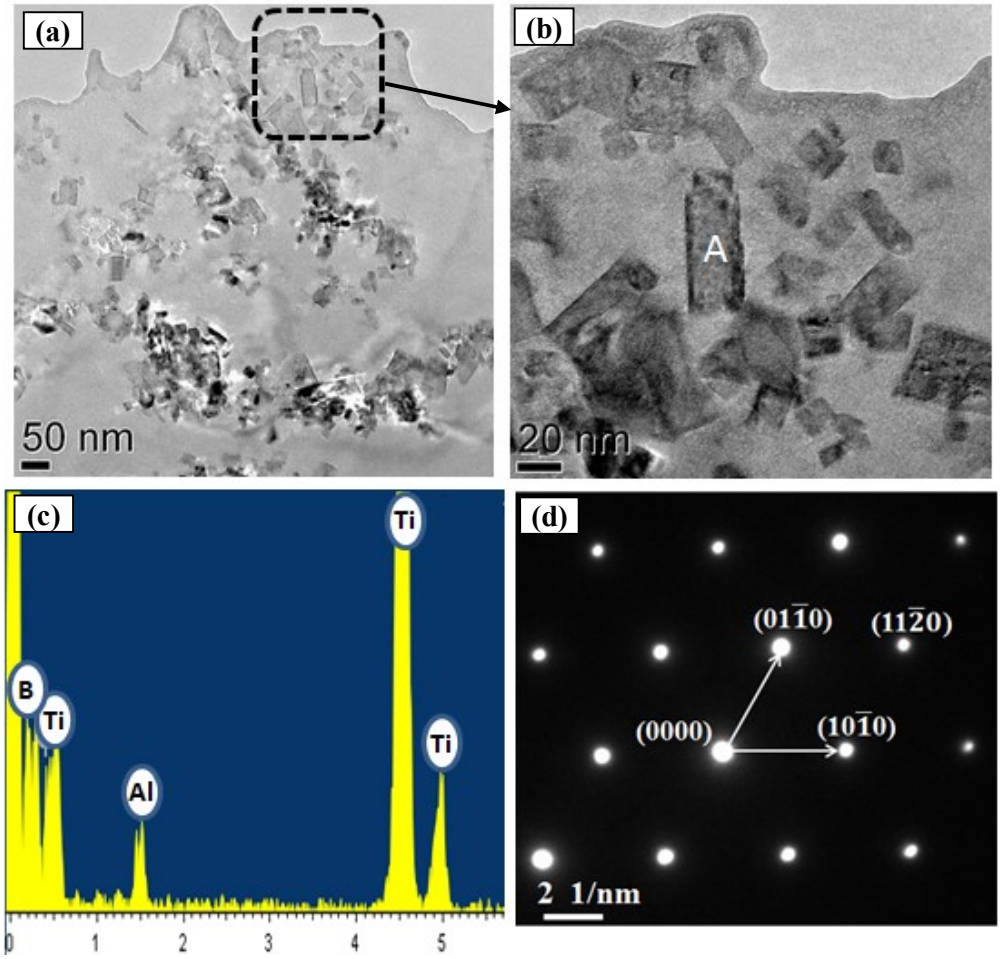

Fig. 3 TEM observations (a, b), EDS results (c) and SADP (d) of TiB_2 nanoparticles in as-cast Alloy T30

During solidification, TiB_2 nanoparticles have a great tendency to segregate in the interdendrite grain boundaries [9]. Using this feature, it is expected to have less DFZ in Alloys T15 and T30 after the peak precipitation heat treatment (375°C/48h). As an example, the microstructure of Alloys B and T30 after heat-treatment is shown in Fig. 4 with the

distribution of intermetallics, nanoparticles, dispersoids and DFZ. As general, the dispersoids precipitated in α-Al cell/grains while the DFZ formed in the interdendritic regions surrounding with the intermetallics. Figs. 4a and 4b show the similar characters of dispersoids in both Alloys B and T30, which are uniformly precipitated in α-Al matrix. This is also confirmed by the TEM observation of dispersoids zone in Fig. 4c and Fig. 4d.

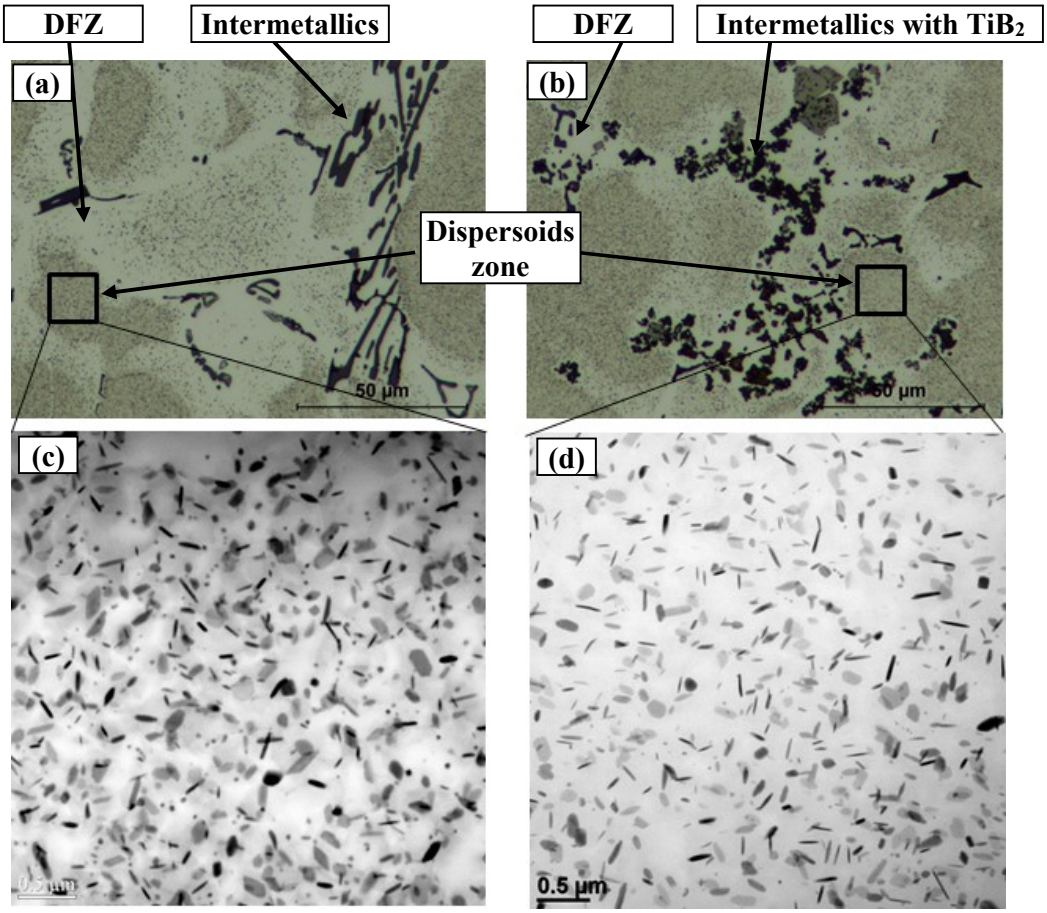

Fig. 4 Distribution of dispersoids and DFZ in Alloy B (a, c) and Alloy T30 (b, d) after 375°C/48h

Table 2 summarizes the characters of dispersoids as well as DFZ of experimental alloys after heat treatment. As shown in Table 2, the average size of dispersoids in three experimental alloys is all in the range of 70-75 nm. However, major difference of the DFZ volume fraction can be found between three alloys. As shown in Fig. 4b, though the DFZ still can be observed in Alloy T30, its volume fraction has been reduced due to the presence of TiB_2 nanoparticles in the interdendrite regions. It is also displayed in Table 2 that the volume fraction of DFZ has been decreased from 31 vol. % in Alloy B to 26 vol. % in Alloy T15 and further to 19 vol. % in Alloy T30. According to the Eq. (1), the calculated volume

fraction of dispersoids increases due to the decreasing volume fraction of DFZ with the addition of TiB2 nanoparticles. The volume fraction of dispersoids raises from 2.54 vol. % in Alloy B to 2.71 vol. % in Alloy T15 and further to 2.96 vol. % in Alloy T30 (Table 2).

Table 2 Characteristics of dispersoids and DFZ in experimental alloys after 375°C/48h

Alloy	Dispersoids		DFZ
	D, nm	V_d, vol.%	V_{DFZ}, vol.%
B	73 ± 12	2.54 ± 0.58	31 ± 8
T15	75 ± 15	2.71 ± 0.75	26 ± 11
T30	71 ± 13	2.96 ± 0.62	19 ± 5

3.2 Evolution of elevated-temperature properties with the addition of TiB_2 nanoparticles

As shown in Fig. 4 and Table 2, the volume fractions of DFZ and dispersoids varied with the addition of TiB_2 nanoparticles after heat treatment. Therefore, different alloy properties are expected. In the present work, the compressive YS at both RT and 300 °C as well as the creep resistance at 300 °C after heat treatment (375°C/48h) have been measured (Fig. 5). As shown in Fig. 5a, it can be seen that the YS increases with the contents of TiB_2 particles at both RT and 300 °C. For instance, YS increased from 101 MPa, 74 MPa in Alloy B to 107 MPa, 78 MPa in Alloy T15 and further to 120 MPa and 84 MPa at RT and 300 °C, respectively, which is 20% at RT and 13% at 300 °C of strength improvement with the addition of 3% of TiB_2 nanoparticles relative to the base alloy. Therefore, the improvement on strength confirms the positive influence of TiB_2 nanoparticles on alloy properties at both RT and elevated temperature.

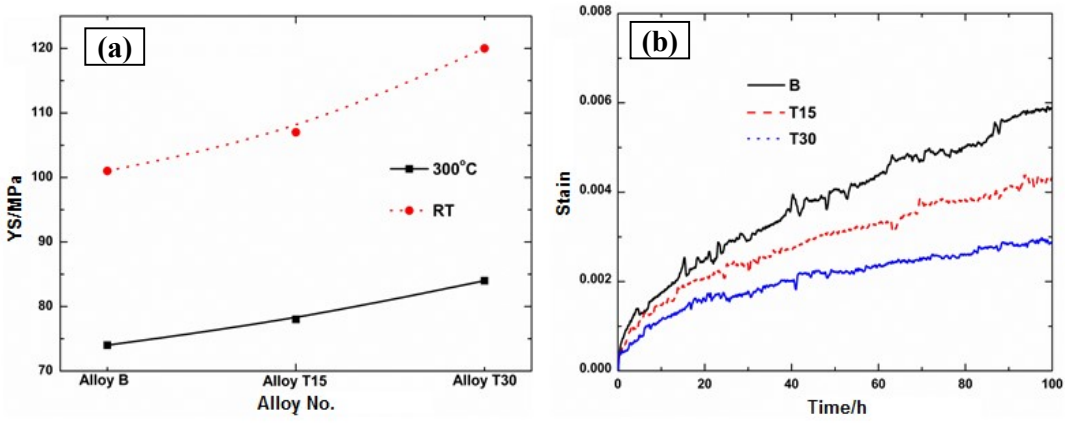

Fig. 5 YS both RT and 300 °C (a) and creep curves at 300 °C (b) after 375°C/48h

As shown in Table 2, the volume fraction of dispersoids increases while the DFZ area decreases with the addition of TiB_2 nanoparticles. Therefore, the strength can be improved due to effectively pinning dislocations by dispersoids according to the Orawan strengthening mechanism [1, 2, 5]. Besides, TiB_2 is reported to an effective grain refiners in aluminum alloys [18]. In the present work, the grain size have been measured using EBSD and results are shown in Fig. 6. It can be found the grain size has been greatly reduced due to addition of TiB_2 nanoparticles. The average grain size is decreased from 356 μm in Alloy B to 122 μm in Alloy T15 and further to 95 μm in Alloy T30. Therefore, the alloy strength can be further improved due to the finer grains in Alloys T15 and T30 according to the Hall-Petch strengthening [19, 20].

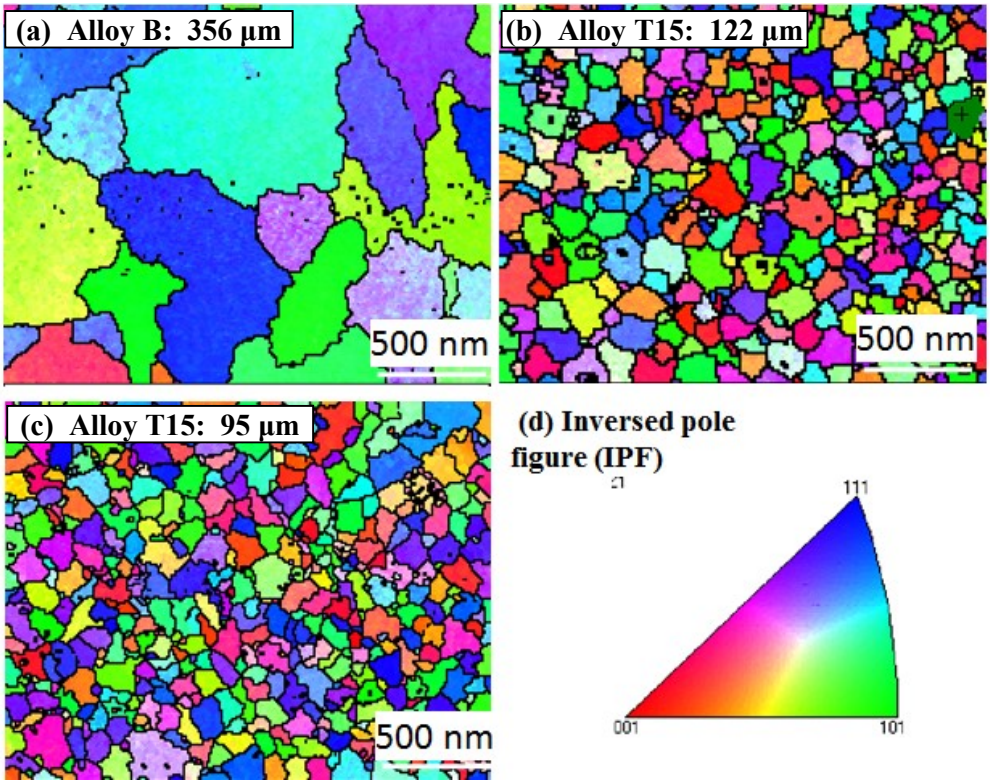

Fig. 6 EBSD mapping results to show the grain size in experimental alloys

Besides, the creep tests at 300 ºC of experimental alloys under a constant load of 38 MPa also have been carried out (Fig. 5b) to show the evolution of creep resistance with the addition of TiB_2. It can be found that the total creep strain in 100 hours decreased with an increasing level of TiB_2 nanoparticles. As shown in Fig. 5b, the total creep strain is decreasing from 0.006 in Alloy B to 0.004 in Alloy T15 and further to 0.003 in Alloy T30, indicating the improvement of creep resistance from the addition of TiB_2 nanoparticles. Moreover, the minimum creep rate $\dot{\varepsilon}$ also descends with increasing addition of TiB_2

nanoparticles. The minimum creep rate is calculated to be 1.1×10^{-8}/s for the base alloy (Alloy B), and it drops to 7.2×10^{-9}/s in Alloy T15 with 1.5% TiB_2 and further decreases to 2.1×10^{-9}/s in Alloy T30 with addition of 3% TiB2 nanoparticles. The minimum creep rate of Alloy T30 is 5 times lower than the base alloy (Alloy B). Similar to the improvement of yield strength from pinning effect of dislocations, the reduced DFZ and higher volume fraction of dispersoids due to the addition of TiB_2 nanoparticles also leads to the better creep properties [2, 3]. However, the finer grain structure caused by TiB_2 addition can reduce the high-temperature creep resistance [21]. It is most likely that TiB_2 nanoparticles in the interdendritic grain boundaries effectively inhibited the motion of grain boundaries. Therefore, the negative influence of finer grains on creep properties has been overcome. The synergistic effect of higher volume fraction of dispersoids and the inhabitation effect on grain boundaries from TiB_2 nanoparticles still results in the improvement of the creep resistance.

In order to better understand the creep behavior of TiB_2 contained materials, the creep tests at different loads were performed to determine two important creep parameters, namely the threshold stress σ_{th} and true stress exponent n [22]. The threshold stress σ_{th} is calculated as a stress value when the minimum creep rates ($\dot{\varepsilon}$) at different loads are extrapolated to 10^{-10} s^{-1}, below which the creep is experimentally not measurable. The true stress exponent n is the slope of $\ln\dot{\varepsilon}$ -$\ln(\sigma-\sigma_{th})$ curve [23]. The calculated results are shown in Fig. 7. As shown in Fig. 7a, the minimum creep rate $\dot{\varepsilon}$ decreases with the increasing addition of TiB_2 nanoparticles at all applied loads and the threshold stress σ_{th} increases from 22.4 MPa in Alloy B to 24.2 MPa in Alloy T30. It is reported that an increase of 3 MPa in threshold stress translates into an order of magnitude decrease in the minimum creep rate [24]. In the present work, the minimum creep rate has been decreased 5 times with an increase of threshold stress of 1.8 MPa, confirming an overall positive influence of TiB_2 nanoparticles on creep resistance. Besides, the true stress exponent n is calculated to close 3 for all 3 experimental alloys (Fig. 7b), which suggests the creep is still controlled by dislocation glide mechanism rather than the grain boundaries [25], further confirming that the motion of grain boundaries has been effectively restricted by the TiB_2 nanoparticles distributed in interdendrite regions.

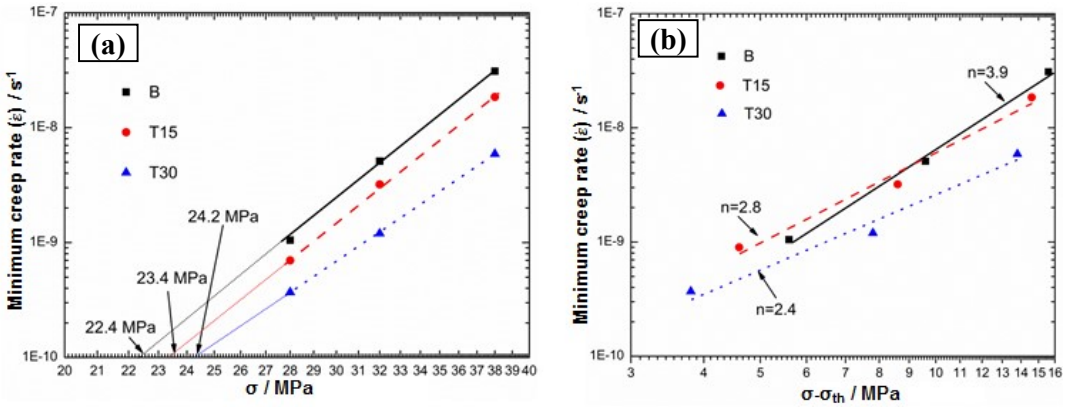

Fig. 7 Calculation of threshold stress σ_{th} (a) and true stress exponent n (b) after 375°C/48h

As shown in Figs. 5 and 7, the elevated-temperature properties, such as the yield strength and creep resistance, have been increased due to TiB_2 nanoparticles, which results in a strong pinning effect on dislocations and effective inhibition on the grain boundary motion. A superior YS (84 MPa) and excellent creep resistance (2.1×10^{-9}/s of minimum creep rate) at 300 °C have been achieved with 3% TiB_2 addition, providing a novel possibility to further improve the properties of Al-Mn-Mg 3xxx alloys for elevated-temperature applications.

4. Conclusions

In the present work, the distribution of TiB_2 particles and their influence on elevated-temperature properties in Al-Mn-Mg 3004 alloy has been investigated and the following conclusions can be obtained:

(1) TiB_2 nanoparticles have been successfully incorporated into aluminum and during solidification those particles are mainly distributed in the interdendritic regions with a size range of 20-80 nm.

(2) Lower volume fraction of dispersoid free zone and finer grain size due to the addition of TiB_2 nanoparticles result in the higher strength at both RT and 300 °C. In heat-treated alloy containing 3% TiB_2, the yield strengths have been improved by 20% and 13% at room temperature and 300 °C, respectively, relative to the base alloy free of TiB_2.

(3) The creep resistance at 300 °C also increases with the addition of TiB_2 nanoparticles. Compared to the base alloy free of TiB_2, the minimum creep rate has been reduced 5 times with an increase of 1.8 MPa in the threshold stress in the alloy with 3% TiB_2.

Acknowledgement

The authors would like to acknowledge the financial support from the Natural Sciences and Engineering Research Council of Canada (NSERC) and Rio Tinto, through the NSERC Industry Research Chair in Metallurgy of Aluminum Transformation at University of Quebec at Chicoutimi.

References

[1] LI Y J, MUGGERUD A M F, OLSEN A, FURU T Precipitation of partially coherent α-Al(Mn,Fe)Si dispersoids and their strengthening effect in AA 3003 alloy [J]. Acta Mater., 2012, 60: 1004-1014.

[2] LIU K, CHEN X G Development of Al–Mn–Mg 3004 alloy for applications at elevated temperature via dispersoid strengthening [J]. Mater. Des., 2015, 84: 340-350.

[3] LIU K, CHEN X G Evolution of Intermetallics, Dispersoids, and Elevated Temperature Properties at Various Fe Contents in Al-Mn-Mg 3004 Alloys [J]. Metall. Mater. Trans. B, 2015, 1-10.

[4] HUANG H-W, OU B-L Evolution of precipitation during different homogenization treatments in a 3003 aluminum alloy [J]. Mater. Des., 2009, 30: 2685-2692.

[5] MUGGERUD A M F, M RTSELL E A, LI Y, HOLMESTAD R Dispersoid strengthening in AA3xxx alloys with varying Mn and Si content during annealing at low temperatures [J]. Mater. Sci. Eng., A, 2013, 567: 21-28.

[6] LI Y J, ARNBERG L Quantitative study on the precipitation behavior of dispersoids in DC-cast AA3003 alloy during heating and homogenization [J]. Acta Mater., 2003, 51: 3415-3428.

[7] LÜ X-y, GUO E-j, ROMETSCH P, WANG L-j [J]. Trans. Nonferrous Met. Soc. China, 2012, 22: 2645-2651.

[8] KENNEDY A R, KARANTZALIS A E, WYATT S M The microstructure and mechanical properties of TiC and TiB2-reinforced cast metal matrix composites [J]. J. Mater. Sci., 1999, 34: 933-940.

[9] NABAWY A M, CHEN X-G Fabrication of Al-TiB2 Nanocomposites by Flux-Assisted Melt Stirring [J]. Metall. Mater. Trans. B, 2015, 46: 1596-1602.

[10] IIZUKA T, OUYANG Q-b Microstructures and mechanical properties of MgAl2O4 particle-reinforced AC4C aluminum composites [J]. Trans. Nonferrous Met. Soc. China, 2014, 24: 2337-2345.

[11] LIU B, HUANG W-m, WANG H-w, WANG M-l, LI X-f Compressive behavior of high particle content B4C/Al composite at elevated temperature [J]. Trans. Nonferrous Met. Soc. China, 2013, 23: 2826-2832.

[12] TJONG S C, MA Z Y The high-temperature creep behaviour of aluminium-matrix composites reinforced with SiC, Al2O3 and TiB2 particles [J]. Compos. Sci. Technol., 1997, 57: 697-702.

[13] LIU P X, LIU Y, XU R Microstructure quantitative analysis of directionally solidified Al-Ni-Y ternary eutectic alloy [J]. Trans. Nonferrous Met. Soc. China, 2014, 24: 2443-2451.

[14] MUGGERUD A M F, LI Y, HOLMESTAD R Composition and orientation relationships of constituent particles in 3xxx aluminum alloys [J]. Philosophical Magazine, 2014, 94: 556-568.

[15] QIU F, HAN Y, CHENG A, LU J, JIANG Q Effect of Cr Content on the Compression Properties and Abrasive Wear Behavior of the High-Volume Fraction (TiC–TiB2)/Cu Composites [J]. Acta Metall. Sin. (Eng. Lett.), 2014, 27: 951-956.

[16] TANG W-m, ZHENG Z-x, WU Y-c, WANG J-m, LÜ J, LIU J-w Synthesis of TiB2 nanocrystalline powder by mechanical alloying [J]. Trans. Nonferrous Met. Soc. China, 2006, 16: 613-617.

[17] BISWAS K, BASU B, SURI A K, CHATTOPADHYAY K A TEM study on TiB2–20%MoSi2 composite: Microstructure development and densification mechanism [J]. Scr. Mater., 2006, 54: 1363-1368.

[18] MOHANTY P S, GRUZLESKI J E Mechanism of grain refinement in aluminium [J]. Acta Metall. Mater., 1995, 43: 2001-2012.

[19] HANSEN N The effect of grain size and strain on the tensile flow stress of aluminium at room temperature [J]. Acta Metall., 1977, 25: 863-869.

[20] LAI J, ZHANG Z, CHEN X G The thermal stability of mechanical properties of Al–B4C composites alloyed with Sc and Zr at elevated temperatures [J]. Mater. Sci. Eng., A, 2012, 532: 462-470.

[21] HIRATA T, OSA T, HOSOKAWA H, HIGASHI K Effects of flow stress and grain size on the evolution of grain boundayr microstructure in superplastic 5083 aluminum alloy [J]. Mater. Trans., 2002, 43: 2385-2391.

[22] TIAN J, SHI Z-q Creep mechanism and creep constitutive model of aluminum silicate short-fiber-reinforced magnesium matrix composite [J]. Trans. Nonferrous Met. Soc. China, 2014, 24: 632-640.

[23] LI Y, LANGDON T G A simple procedure for estimating threshold stresses in the creep of metal matrix composites [J]. Scr. Mater., 1997, 36: 1457-1460.
[24] FARKOOSH A R, CHEN X G, PEKGULERYUZ M Interaction between molybdenum and manganese to form effective dispersoids in an Al–Si–Cu–Mg alloy and their influence on creep resistance [J]. Mater. Sci. Eng., A, 2015, 627: 127-138.
[25] LI Y, NUTT S R, MOHAMED F A An investigation of creep and substructure formation in 2124 Al [J]. Acta Mater., 1997, 45: 2607-2620.

TiB_2纳米颗粒对Al-Mn-Mg 3004 合金中高温性能的影响

刘 坤，A. M. Nanawy, X.–G. Chen
Department of Applied Science，University of Quebec at Chicoutimi，
Saguenay, QC, Canada, G7H2B1

摘要：

为了研究TiB2纳米颗粒对Al-Mn-Mg 3004合金中高温性能的影响，不同含量的TiB_2纳米颗粒（1.5 wt. % 和3 wt.%）分别加入3004 合金。透射电镜和X射线衍射结果表明TiB_2纳米颗粒主要分布在枝晶界，尺寸在20-80 nm。因此，合金中弥散相无析出带的体积分数大幅减少。同时，TiB_2纳米颗粒的添加有效钉扎了晶界和位错的移动，从而提高了合金的性能。在经过峰值析出热处理后，与未添加TiB_2纳米颗粒的合金相比，加入3% TiB_2纳米颗粒的3004 合金在常温和300 ºC下的屈服强度分别提高了20%和13%。同时，该合金在300 ºC下的最小蠕变速率也降低了5倍，体现了TiB_2纳米颗粒对Al-Mn-Mg合金中高温性能的强化作用。

关键词：Al-Mn-Mg 3004 合金； TiB_2纳米颗粒； 弥散相无析出带；中高温性能；蠕变。